ChemPubSoc Europe

DOI: 10.1002/cctc.201701841

CHEMCATCHEM Full Papers

Structure-Sensitive Scaling Relations: Adsorption Energies from Surface Site Stability

Luke T. Roling[b] and Frank Abild-Pedersen*[a]

The design of heterogeneous catalysts is accelerated by the identification of thermochemical reactivity descriptors, which enable the prediction of promising materials through efficient screening. Motivated by previous discoveries of linear scaling relations between the adsorption energies of related atoms and molecules, we present a new scaling between the adsorption energies of metal atoms and metal–adsorbate complexes, which can be used to directly predict catalytically relevant molecular adsorption energies. In contrast to existing models based on the coordination number of surface atoms alone, our model can predict adsorption energies with site-by-site resolution considering local structural effects and also has potential extensions to include contributions of neighboring metal identity in alloy systems. Integration of this scaling with a previously identified model for metal–metal interactions enables the accurate prediction of molecular adsorption energies on nanoparticles by performing only a small set of slab-based calculations.

Introduction

The design of improved heterogeneous catalysts requires the reliable prediction of reaction energetics in a vast design space, motivating the development of accurate and efficient methods for screening and identifying promising materials.[1] Computational tools enable atomic-scale investigations of materials properties, including the manipulation of catalyst composition and surface structure toward the goal of identifying and synthesizing materials with properties optimized for a particular catalytic reaction.[2,3] The discovery of promising materials is aided by the identification of thermochemical reactivity descriptors, which enable rapid screening of materials that exhibit desirable electronic band structure properties leading to favorable adsorption energies of atomic or molecular species.[4–6] Previous studies have shown that the adsorption strength of atoms and molecules correlates with the coordination number of the surface site to which the adsorbate binds, but that coordination number alone is generally insufficient to describe adsorption on nanoparticles.[7–9] More recent works have introduced corrections such as the "generalized coordination number"[10,11] or the "orbitalwise coordination number"[12] to extend the coordination-based approach to introduce structure-sensitive dependence into relationships between metal atom coordination and molecular adsorption strength. All of these relationships are based on the foundation that atoms with higher coordination have stabilized d-states that subsequently interact more weakly with adsorbate molecules with increasing metal–metal coordination.[6,13] However, these approaches lack clear extensions into bimetallic compositional space, which is critical for the design of alloy catalysts with optimized catalytic activity.

In this work, we show how structure sensitivity can be incorporated directly into a traditional scaling approach without introducing gradually changing coordination numbers. Our model is formulated based on a similar premise as those based on metal coordination alone, anticipating that metal atoms that are more strongly bound to a surface should interact less strongly with adsorbates. We therefore establish a relationship between adsorbate binding energies and the stability of individual metal surface sites, which serves as a continuous activity descriptor. Consequently, adsorbate binding energies can be predicted from the binding energy of single metal atoms, thus enabling catalyst design through manipulation of the metal site stability (e.g., through varying local structure and atomic composition). We apply this method to predict adsorption energies on nanoparticle models with a range of surface adsorption sites. We finally show that this approach can be coupled with a recently derived model for metal–metal interactions, enabling the prediction of adsorption energies on nanoparticles based only on simple sets of slab-based calculations.

Results and Discussion

In the following, we will address structure sensitivity in heterogeneous catalysis by using an approach based entirely on linear scaling relations. For transition-metal surfaces, it has been shown that the binding energy of molecular species (e.g., XH_y) and the binding energy of the atom (X) through

[a] Dr. F. Abild-Pedersen
SUNCAT Center for Interface Science and Catalysis
SLAC National Accelerator Laboratory
2575 Sand Hill Road, Menlo Park, CA 94025 (USA)
E-mail: abild@slac.stanford.edu

[b] Dr. L. T. Roling
SUNCAT Center for Interface Science and Catalysis
Stanford University
443 Via Ortega, Stanford, CA 94305 (USA)

Supporting information and the ORCID identification number(s) for the author(s) of this article can be found under: https://doi.org/10.1002/cctc.201701841.

which the adsorbate binds to the surface scale linearly with each other, as was observed for the binding energies of CH_y/C, NH_y/N, OH/O, and SH/S pairs.[14] These linear correlations hold between adsorbates on surfaces with similar structure, in which the slope is surface structure independent and all structural information is contained in the constant intercept.[15] It is also known that within a single metal, binding energies change linearly with variations in metal–metal coordination or shift in metal d-band center.[16,17] This suggests that similar linear relationships between the binding energy of a metal–adsorbate complex (M–A) to a surface and the binding energy of the metal atom (M) to a surface should exist.

To investigate this potential scaling, we use several energetic quantities in our analysis. We calculate the binding energy of species X (ΔE_X) to a surface as the difference in total energy between the surface with X adsorbed (E_{S-X}) and the isolated surface (E_S) and gas-phase X ($E_{X(g)}$). We are interested in identifying relationships between two quantities: the binding energy of a metal atom (ΔE_M) to a surface and the binding energy of a complex of an additional adsorbate with the metal atom (ΔE_{M-A}) to the same surface. We accordingly define these quantities as Equations (1) and (2):

$$\Delta E_M = E_{S-M} - E_S - E_{M(g)} \quad (1)$$

$$\Delta E_{M-A} = E_{S-M-A} - E_S - E_{M-A(g)} \quad (2)$$

We look for a linear scaling relationship between these quantities for a given metal and adsorbate, which assumes the form in Equation (3):

$$\Delta E_{M-A} = \alpha_{M-A}\Delta E_M + \beta_{M-A} \quad (3)$$

for some parameters α_{M-A} and β_{M-A}.

To understand the relationship between these two quantities, we performed density functional theory (DFT) calculations of single metal atom adsorption on face centered cubic (fcc) (111), fcc (100), and fcc (211) surfaces of the same metal. We varied the coordination number of the metal atom by changing the metal atom coverage of the topmost surface layer of the slab on which the metal atom adsorbs. This yields a substantial range of metal binding energy values, corresponding to metal atom coordination numbers ranging between 3 (adatom on a (111) surface) and 9 (atom in a (111) surface) in 13 unique adsorption configurations. Notably, we did not observe any substantial reconstruction of surfaces (or nanoparticles, in later models) owing to addition or removal of any metal atoms in this study, that is, the fcc stacking was well-preserved when adding or removing metal atoms. We then performed adsorption calculations for OH, CH_3, and CO, representing three intermediates relevant in a broad range of catalytic applications,[18–22] in the on-top position on these metal adatoms. All binding energies calculated in this study are tabulated in Tables S1–S11 in the Supporting Information. Illustrations of the surface configurations highlighting the arrangement of the coordinating metal atom and the adsorbate are provided in Figure 1. The adsorbate surface coverages in this study are relatively low (0.25 ML or less), so adsorbate–adsorbate interactions are negligible. Notably, additional work will be needed to determine the applicability of this proposed scheme at higher coverages characteristic of many catalytic systems owing to the complex nature of adsorbate–adsorbate interactions.

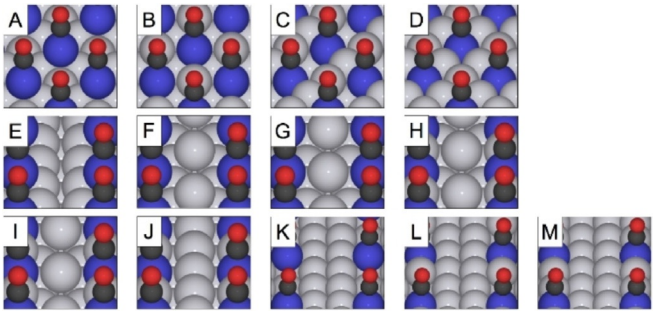

Figure 1. Adsorption structures for the determination of ΔE_{M-CO} and ΔE_{CO}. An adsorbate molecule binds atop a metal atom (blue) with varying coordination number (CN) to other metal atoms (grey): (A) CN = 3, fcc(111); (B) CN = 5, fcc(111); (C) CN = 7, fcc(111); (D) CN = 9, fcc(111); (E) CN = 4, fcc(100); (F) CN = 4, fcc(100); (G) CN = 6, fcc(100); (H) CN = 6, fcc(100); (I) CN = 8, fcc(100); (J) CN = 8, fcc(100); (K) CN = 5, fcc(211); (L) CN = 6, fcc(211); (M) CN = 7, fcc(211). Other atom colors: O (red), C (black).

The relationships between ΔE_{M-A} and ΔE_M for OH, CH_3, and CO adsorption are shown in Figure 2 A–C, respectively, whereas

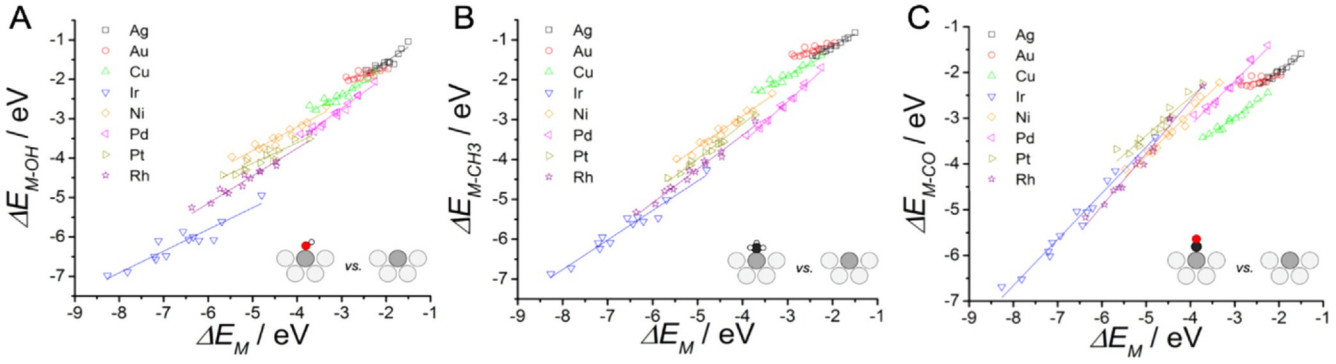

Figure 2. Binding energies of metal–adsorbate complexes plotted against metal atom binding energies for (A) metal–OH, (B) metal–CH_3, and (C) metal–CO. Adsorbate molecules are bound atop metal atoms in the slab calculations. Best-fit lines for a linear relationship within each metal are drawn. Parameters for each linear fit are provided in Table S12 in the Supporting Information.

details of the linear fit parameters are given in Table S12 (in the Supporting Information). These generally demonstrate very strong linear relationships with high correlation coefficients ($R^2 = 0.9$ or higher); a notable exception is observed for Au surfaces, for which the R^2 values are rather low (0.3–0.7) owing to the relatively small slope of the relationship between ΔE_{M-A} and ΔE_M on that metal. Still, the magnitude of the scatter around the best-fit line is small despite the poor correlation coefficient.

We have established a relationship between ΔE_M and ΔE_{M-A}; a related quantity is the binding energy of the adsorbate itself (ΔE_A) to the surface (including the additional metal atom, which was previously treated as a separate adsorbate), which can be a useful predictor of catalytic activity. The binding energy of the adsorbate is given by Equation (4):

$$\Delta E_A = E_{S-M-A} - E_{S-M} - E_{A(g)} \quad (4)$$

Utilizing the linear scaling established between ΔE_{M-A} and ΔE_M [Eq. (3)] and substituting into Equation (4), we obtain Equation (5):

$$\Delta E_A = (\alpha_{M-A} - 1)\Delta E_M + (\beta_{M-A} + C) \quad (5)$$

in which $C = E_{M-A(g)} - E_{M(g)} - E_{A(g)}$ is the reaction energy between the metal atom and the adsorbate in the gas phase. We therefore anticipate a linear relationship between ΔE_A and ΔE_M, and plot these quantities in Figure 3 for all three adsorbates along with the best-fit lines for each metal (best-fit parameters are given in Table S13 in the Supporting Information). The slope for each relationship between adsorbate and metal binding energy can be obtained directly from the linear relationship between ΔE_M and ΔE_{M-A}, as given by Equation (5). Notably, for relationships between ΔE_{M-A} and ΔE_M for which α_{M-A} is nearly 1, the slope of the relationship between ΔE_A and ΔE_M is close to 0, implying little to no change in adsorbate energy despite possibly significant changes in the binding energy of the metal atom. This is seen, for example, for adsorption of CO on Pd, in which the slope of the relationship between ΔE_{Pd-CO} and ΔE_{Pd} is 0.97, which leads to a near zero slope for the relationship between ΔE_{CO} and ΔE_{Pd} as seen in Figure 3C. This negligible slope leads to essentially no correlation between ΔE_{CO} and ΔE_{Pd}. In contrast, the relationship between ΔE_{Au-CO} and ΔE_{Au} has a low slope of 0.18, and ΔE_{CO} therefore exhibits very strong dependence on ΔE_{Au} (slope 0.82). We observe that the slopes of these relationships depend on both adsorbate identity and metal identity. Although it is difficult to disentangle these effects owing to the limited data size of the present study, a future systematic study of how the metal–adsorbate slope changes as a function of adsorbate type would yield valuable physical insights.

The correlation coefficients for the relationships between ΔE_A and ΔE_M are markedly weaker (0.0–0.9) than those for the relationships between ΔE_{M-A} and ΔE_M, particularly owing to the relatively small slopes of many of the relationships shown in Figure 3. However, the adsorbate binding energies are still well-treated by the respective linear relationships, with average mean absolute errors (MAEs) of 0.08 eV, 0.06 eV, and 0.08 eV for OH, CH_3, and CO, respectively. In the Supporting Information, we present a comparison of the prediction of adsorption energies calculated in this study by using traditional coordination number, generalized coordination number, and metal atom binding energy as descriptors. The quality of the linear fits, as well as the errors in calculated adsorption energies, are fairly consistent between all three approaches: standard coordination number has MAEs of 0.06 eV, 0.05 eV, and 0.07 eV for OH, CH_3, and CO; generalized coordination number yields MAEs of 0.05 eV, 0.05 eV, and 0.07 eV (details in Figures S1–S3 in the Supporting Information). Although these approaches show marginally reduced error in predicting adsorption energies, our approach offers possible future extensions into the design space of manipulating metal atom identities in alloy systems, which is not possible to account for by using coordination number alone as a descriptor. We also find the continuous binding energy descriptor to be more intuitive from a physical perspective than a scale utilizing non-integer, normalized coordination numbers.

Molecular adsorbates in catalytic processes are not restricted to adsorption in the on-top position. To investigate how our approach might be extended to describe adsorption in other sites, we performed an additional set of calculations of CO adsorption (as the highest error adsorbate in the on-top calculations) in bridge sites on model surfaces. In this case, we evalu-

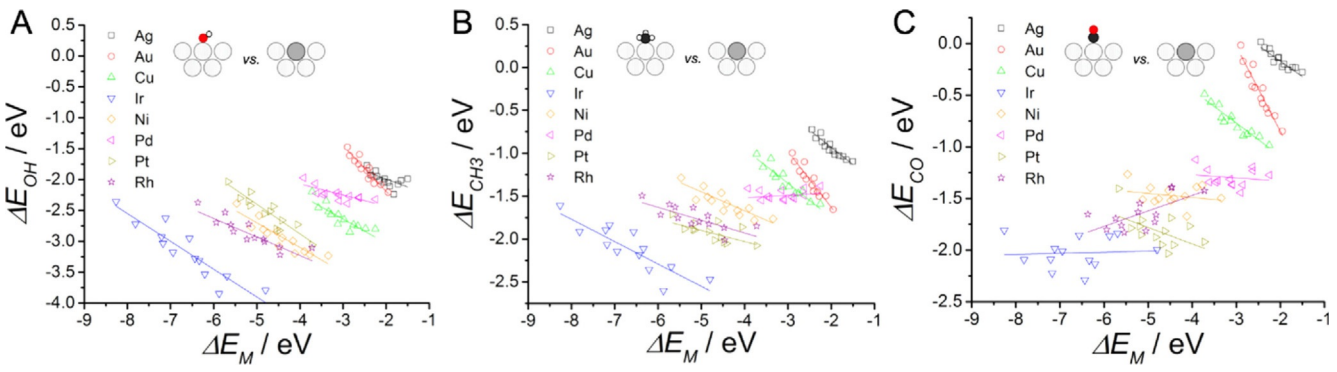

Figure 3. Binding energies of adsorbates plotted against the binding energy of the metal atom to which they bind, for adsorbates (A) OH, (B) CH_3, and (C) CO. Best-fit lines for a linear relationship within each metal are shown. Parameters for each linear fit are provided in Table S13 in the Supporting Information.

ated the binding energy of metal dimers to the catalyst surface and plotted these values against the respective CO binding energies in Figure 4. By varying the local coordination environment of the metal dimers within the unit cell, we obtained a total of eight data points per metal (three on (111) and (100) surfaces, and two on (211) surfaces). We again found a linear relationship between these quantities, demonstrating that this method is not limited to on-top adsorption. The MAE around the best-fit lines was 0.05 eV, which is equivalent to the MAE calculated by using the generalized coordination number approach for bridge adsorption. In the absence of a clear definition of standard coordination number for bridge sites, we omit a comparison with those values. Notably, the relationships for all metals exhibit a negative slope between the metal dimer and CO binding energies, in contrast to the top-bound case in which very flat/uncorrelated relationships were found (for Ir, Ni, Pd, and Rh in particular). This suggests that the binding mechanism of CO is changing between the sites; the fine details of this phenomenon are outside the scope of this study, but the poor correlation seen in Figure 3C (and in the generalized/standard coordination approaches) between CO and certain metals likely relates to a CO binding mode that is relatively independent of the environment of the metal atom to which it binds and therefore cannot be captured by using these classes of adsorption models.

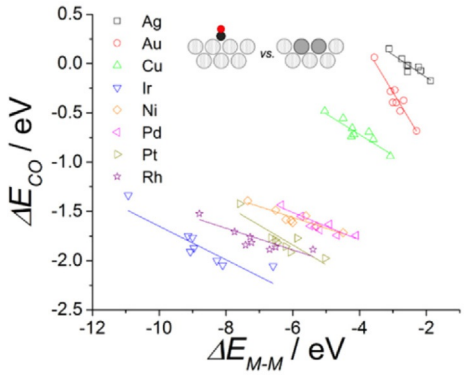

Figure 4. Binding energy of CO in the bridge site plotted against the binding energy of the metal–metal dimer to which they bind. Best-fit lines for a linear relationship within each metal are shown. Parameters for each linear fit are provided in Table S13 in the Supporting Information.

Our approach offers the ability to predict binding energies with site-by-site resolution on catalysts exposing a variety of adsorption sites. To briefly evaluate the predictive power of our approach, we tested our simple model against full-scale DFT calculations of CO adsorption, which exhibited the weakest linear correlations in the slab-based models, on 147-atom cuboctahedral nanoparticles of Ag, Au, Cu, Ir, Pd, Pt, and Rh (omitting Ni from this analysis owing to the high cost and complexity of spin-polarized nanoparticle calculations). These 147-atom particles expose four unique types of surface atoms: one on the (100) facet, one on the (111) facet, an edge atom, and a vertex atom (Figure 5A). We found that the binding energy of each of these atoms to the cluster was a reliable predictor of the binding energy of CO atop each atom type: the mean absolute error for predicting the 28 adsorption energies was 0.12 eV (Figure 5B).

We also performed explicit calculations of CO binding to nanoparticle bridge sites, noting that six unique bridges are present on the monometallic nanoparticles (drawn with filled and unfilled black bars in Figure 5A). We focused first on the CO–Ir system to establish a possible upper bound for our model's error, as CO was the highest error adsorbate and Ir the highest error metal in our previous analyses. The data for the six Ir bridge adsorptions are shown in Figure 5C. Four are predicted with small errors (0.10 eV or less), corresponding to filled black bars shown in Figure 5A: adsorption along the edge (orange-orange and orange-yellow) and adsorption normal to the (100) plane (cyan-cyan and cyan-orange). However, the remaining two data points are poorly described (error 0.4–0.5 eV), corresponding to severe overprediction of binding energies for CO adsorbed perpendicular to the (111) facet. We briefly evaluated OH adsorption on all six Ir bridge sites, and

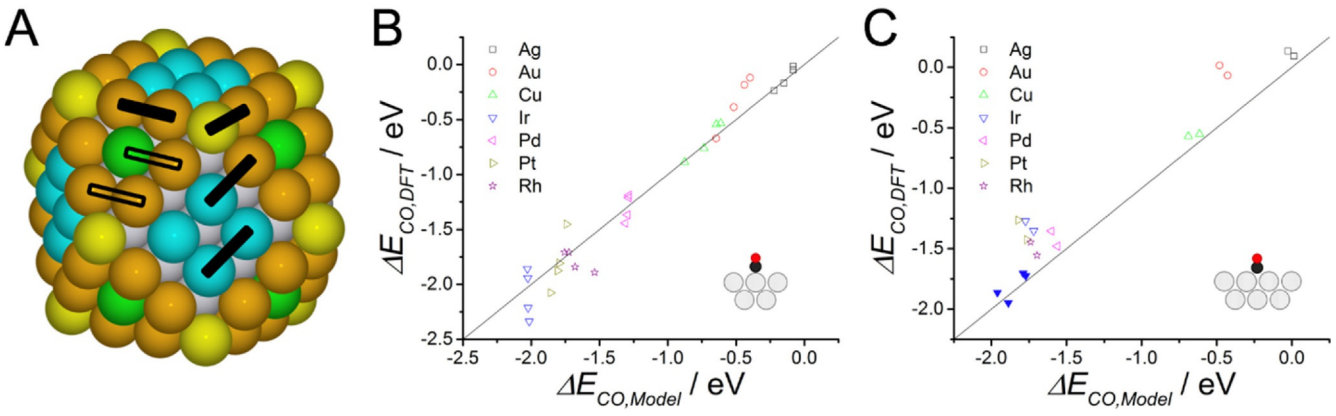

Figure 5. (A) Illustration of different surface sites on a 147-atom cuboctahedral nanoparticle. Atoms are color-coded by their coordination number: fivefold vertex (yellow), sevenfold edge (orange), eightfold (100) facet (cyan), ninefold (111) facet (green). Subsurface atoms are shown in gray. Six unique bridge adsorption sites are shown by the black bars; unfilled bars correspond to the (111)-facet sites investigated in more detail. (B, C) Comparison of ΔE_{CO} predicted by the slab-based scaling relations with that obtained from full-scale DFT calculations for (B) on-top adsorption, and (C) bridge adsorption. Data for the filled-bar bridge sites in (A) are evaluated for Ir only, and correspond to the solid symbols in (C).

found that all sites are described equally well/poorly as for CO adsorption. Moreover, evaluation of these (111)-like binding energies on other fcc metals (Figure 5C) shows that the error is particularly pronounced for the 5d metals (Au, Ir, Pt) and more modest on the other considered 3d and 4d transition metals. We also observe that the generalized coordination model has even higher error for describing this adsorption (0.33 eV vs. 0.27 eV for the (111)-like sites; see Figure S4 in the Supporting Information), suggesting that some unique phenomenon at these sites substantially impacts the ability of this class of models to make accurate predictions.

We performed additional calculations to understand the nature of these sites and the poor agreement between our model and DFT-calculated adsorption energies. We focused first on the adsorption on a "near-edge" site between a (111)-like atom and an edge atom (green-orange adsorption in Figure 5A). Adsorption in this site approaches one of two limiting cases as nanoparticles become larger. In the first, the (111) facet of the nanoparticle will expose sites that approach binding energies on extended (111) surfaces. Our model predicts CO adsorption on Ir(111) in a larger, 4×4 surface unit cell with high accuracy (error 0.06 eV), confirming that the model will more accurately describe adsorption on (111) terraces as the particle size increases. The other limiting case for this adsorption site involves bridge adsorption near the nanoparticle edge. An additional series of calculations representing increasing sizes of nanoparticle edges (see the Supporting Information) shows that the error approaches 0.15 eV in the limiting case, which is more tolerable for applications of our model and is consistent with the relatively higher error observed for Ir compared with the other metals in this study. We therefore attribute the error on this near-edge site of the 147-atom cuboctahedron to finite-size effects that will resolve in the limit of large particle sizes.

The second, "near-corner" adsorption site consists of two edge atoms bridging across a (111) terrace of the cuboctahedral nanoparticles (orange-orange site with black unfilled bar in Figure 5A). We again performed a series of calculations representing limiting cases for large nanoparticles (see the Supporting Information). In this case, our models did not demonstrate substantial improvement of the CO binding energy with increasing particle size; this effect of destabilizing adsorbates is specifically determined by the geometry of that binding site regardless of particle size. We understand this error and its larger apparent effect on 5d metals by considering both the local geometry and electronic effects of these binding sites. First, this site is composed of two edge metal atoms (though the adsorbate itself is not bound along the nanoparticle edge). These edge metal atoms are more weakly bound than metal atoms on the (111) terrace, which our model predicts should correspond to stronger binding of adsorbates. However, CO is constrained by the geometry of the binding site to bind perpendicular to the (111) surface plane, and therefore cannot adopt the optimal bonding structure of CO molecules adsorbed along a nanoparticle edge. We believe this to be particularly important owing to repulsion effects of the metal d-orbitals on the CO states, which would be substantially more pronounced on 5d metals in agreement with the increased error we observe for those metals in this study.[23]

To investigate this repulsion, we performed three calculations of CO binding on edge models comprising four complete rows of metal atoms in 6×6 surface unit cells of (111) slabs of Cu, Ag, and Au to illustrate the relative effects on 3d, 4d, and 5d metals. In the first calculation, CO was allowed to adsorb in its preferred configuration along the edge (Figure 6A). In the second, we constrained the CO at the edge to relax only perpendicular to the (111) surface (Figure 6B). Finally, we performed the same calculation as in Figure 6B but with one additional metal atom to replicate the near-corner effect seen in the nanoparticle models (Figure 6C). Our results suggest that repulsion from the (111) surface leads to favorable "tilting" of the CO molecule away from that surface: moving from the tilted position to the constrained (111) position requires 0.06, 0.07, and 0.11 eV for the Cu, Ag, and Au surfaces, respectively. This tilting is physically prevented in the near-corner model by the presence of an additional atom; our addition of an extra atom as in Figure 6C contributes an additional repulsion of 0.16, 0.16, and 0.31 eV on Cu, Ag, and Au, respectively. This yields a total of 0.21, 0.23, and 0.42 eV weaker binding for Cu, Ag, and Au, respectively, on this near-corner site than could be potentially realized from binding to two edge atoms in a standard edge configuration, which more closely resembles the binding energy predicted from our dimer adsorption calculations. This combined effect is markedly more pronounced on Au than on Ag and Cu, rationalizing our belief that repulsion

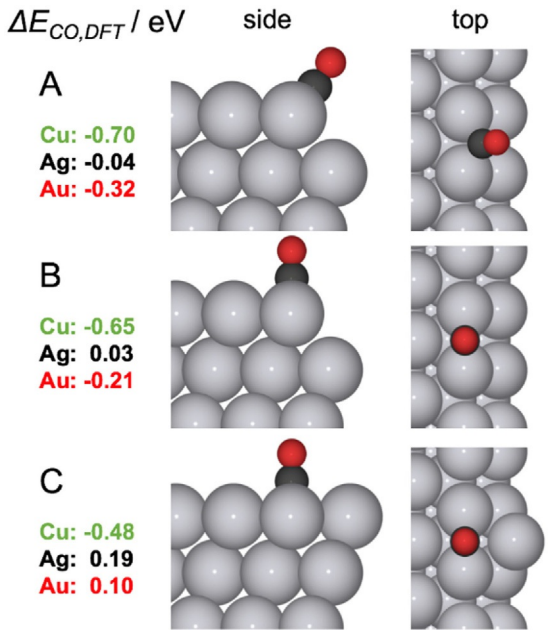

Figure 6. Schematic of models illustrating repulsion effects in 3d, 4d, 5d metals, and respective CO binding energies on each site type. (A) Free "tilted" adsorption of CO at edge sites. (B) CO adsorption constrained to the (111) plane near an edge. (C) CO adsorption in the (111) plan near a corner site. Metal atoms in the periodic image are omitted for clarity (i.e., the second and third layers of metal atoms shown are infinitely repeated in the surface directions as part of a (111) slab).

effects more pronounced on 5d metals limit the CO binding energy to values substantially less than would be typically found for adsorption on two edge atoms.

Notably, both our model and explicit DFT predict these sites have substantially lower adsorbate binding energies than other sites (although with disagreement as to the magnitude of the unfavorability). These therefore represent sites that are less important from a catalytic perspective, as both the model and explicit DFT show that other sites will be strongly preferred. We therefore may not need any direct correction in our model to account for deviations on these specific sites, as activity predictions would be based on sites with stronger binding.

Finally, this model requires metal binding energies as inputs for predicting adsorption energies. Although metal binding energies are inexpensive to calculate in slab models, nanoparticle models with large numbers of binding sites present a particular challenge as the energy of each unique metal site must be independently evaluated to predict adsorption energies of catalytic intermediates. However, we recently published a model for predicting the binding energies of metal atoms by tracking changes in atomic surface coordination, in which similar slab-based calculations were used to parameterize metal–metal interactions and predict binding energies for more complex nanoparticle models.[24] An example of how this model tracks changes in metal atom coordination to predict metal binding energies is provided in the Supporting Information. By coupling this model to the scaling relationship described in this work, we can in principle fully describe the adsorption of catalytic species on generic catalyst structures simply from a base set of slab calculations of metal and adsorbate binding. We evaluated the utility of this combined model using model-predicted metal binding energies as inputs for CO adsorption on nanoparticles. Notably, to do so for our slab-based adsorption calculations would be trivial, as the metal adsorption energies were parameterized with the same set of slab calculations used for molecular adsorption in this present study, and the same fit would be obtained as for the explicitly calculated metal binding energies.

A comparison of the parity plots using the explicit binding energy and combined approaches is shown in Figure 7. The adsorption energies of CO atop metal atoms in nanoparticles is predicted with a MAE of 0.12 eV if using the combined model, which is identical to that calculated by using the explicit binding energy approach shown in Figure 5B. The general agreement between the two models is expected, as the error in predicting the metal binding energies and the slopes of the metal–adsorbate relationships in this study are both relatively small. For the (111)-like bridge binding configurations shown in Figure 5, the combined model predicted bridge-bound CO with a MAE of 0.18 eV, whereas the model using explicit binding energies had a MAE of 0.27 eV. In this case, the model for dimer adsorption overestimates the stability of the dimers (compared with the explicit DFT values) owing to its parameterization on slab-based models rather than on nanoparticles exhibiting compression; this effect is also seen (but less pronounced) for adsorption of single metal atoms in the on-top binding case. This overestimation has a compensatory effect that cancels some of the error in the explicit metal binding approach for bridge binding, as CO is subsequently predicted to absorb more weakly on the combined model. We performed DFT calculations to determine CO binding energies on the remaining bridge sites for all metals considered (without considering the metal dimer binding energies), and found that these non-(111) sites were predicted with a MAE of 0.08 eV if using the combined model.

Overall, the combined approach demonstrates a powerful enhancement of the model presented here, as two small sets of DFT calculations (one for parameterizing metal adsorption energies, and another to define the metal–adsorbate relationship scaling) on slab models can be used to predict adsorption energies in more complex systems (e.g., nanoparticles) with site-by-site resolution. We showed previously that the metal–metal adsorption model was useful for reproducing surface energies and therefore equilibrium nanoparticle shapes.[24] The extension to molecular adsorption energies described in this work should lay a groundwork for future simulations in which changes in preferred nanoparticle structure can be predicted based on molecular adsorption, which is difficult to capture by using coordination numbers alone. This approach will also be particularly useful for bimetallic systems exposing a large number of potential adsorption sites, and motivates the future

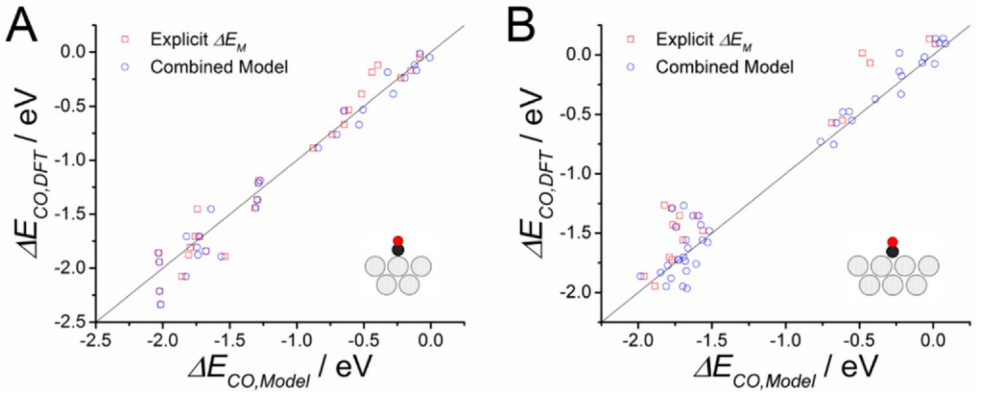

Figure 7. Comparison of predicted CO adsorption energies using the explicit metal binding energy model with a combined approach utilizing predicted metal binding energies for (A) on-top CO adsorption and (B) bridge CO adsorption.

development of relationships for predicting metal adsorption energies in bimetallic systems. The development of these relationships will require care, as they require combining relationships between surface structure and adsorption energies, as studied in this work, with relationships between surface composition and adsorption energies, which have been studied extensively for monometallic and bimetallic systems of fixed surface structure. Bimetallic systems will also yield a wider range of heterogeneous binding sites and adsorption geometries that will require additional consideration. Although such an extension of the present work is non-trivial, the anticipated ability to treat a vast structural and compositional space through straightforward calculations offers great potential for future catalyst design.

Conclusions

We have presented an extension of regular adsorbate scaling relations, in which adsorbate binding energies can be predicted directly from the binding energies of the metal atoms through which they bind. By taking advantage of a natural relationship between the adsorption energies of metal atoms and metal–adsorbate complexes, we show that the binding energy of adsorbates is well represented by a linear function of metal atom stability. We anticipate that our approach will provide a useful tool for improved catalyst design, as the binding energy of a metal atom (and, subsequently, that of the adsorbate) can be directly tuned by identifying and ultimately designing surface sites with specified atomic composition and surface structure, which cannot both be accounted for by using existing coordination-based approaches to predict binding energies.

Computational Methods

Density functional theory (DFT) calculations were performed by using the Quantum ESPRESSO package.[25] The RPBE functional[26] and ultra-soft Vanderbilt pseudopotentials[27] were used. Calculations were performed with a plane-wave cutoff of 500 eV and a density cutoff of 5000 eV. The lattice constants of metals used in this study were optimized to the following bulk values (experimental values[28] in parentheses, all values in Å): Ag 4.22 (4.09), Au 4.20 (4.08), Cu 3.68 (3.61), Ir 3.88 (3.84), Ni 3.55 (3.52), Pd 3.98 (3.89), Pt 3.99 (3.92), Rh 3.85 (3.80). Calculations on the (111) and (100) surfaces of fcc transition metals were performed on slabs with a $2\times2\times6$ unit cell, with the top two layers allowed to relax. Calculations on the (211) surfaces were performed in a $1\times3\times12$ unit cell, with the top six layers allowed to relax. The dipole correction to the total energy was included for surface calculations.[29] The relaxation of the coordinating atom of the adsorbate (i.e., C for CO and CH_3, and O for OH) was constrained to the direction normal to the (111) and (100) surfaces and normal to the (211) step edge to ensure no movement from the considered on-top and bridge sites; other atoms in the adsorbate (e.g., H) were allowed to freely relax. A $6\times6\times1$ Monkhorst–Pack *k*-point mesh[30] was used for the (111) and (100) surfaces, and a $4\times4\times1$ mesh was used for the (211) surfaces. Calculations in the larger 6×6 surface unit cell of (111) surfaces (i.e., surface edge model) were performed with three complete layers and one partial layer of metal atoms; the bottom two layers were fixed and the energy was sampled with a $2\times2\times1$ *k*-point mesh. At least 10 Å of vacuum separated successive slabs in the *z*-direction. Calculations involving 147-atom cuboctahedral nanoparticles were performed with all atoms relaxed; the adsorbate molecule was constrained to move normal to the respective surfaces/edges of the nanoparticle on which it adsorbed to ensure it remained on the considered on-top and bridge sites. Nanoparticle calculations were performed by using only the gamma point, and at least 10 Å of vacuum separated successive nanoparticles in all directions. All geometry optimizations were performed until forces on relaxed atoms were less than 0.02 eV $Å^{-1}$. Calculations with Ni were performed spin-polarized.

Acknowledgments

We acknowledge support from the U.S. Department of Energy, Office of Basic Energy Sciences, to the SUNCAT Center for Interface Science and Catalysis at SLAC National Accelerator Laboratory and Stanford University.

Conflict of interest

The authors declare no conflict of interest.

Keywords: coordination number · density functional theory · heterogeneous catalysis · nanoparticles · transition metals

[1] T. Bligaard, J. K. Nørskov, S. Dahl, J. Matthiesen, C. H. Christensen, J. Sehested, *J. Catal.* **2004**, *224*, 206–217.
[2] F. Zaera, *Chem. Soc. Rev.* **2013**, *42*, 2746–2762.
[3] C. J. Cramer, D. G. Truhlar, *Phys. Chem. Chem. Phys.* **2009**, *11*, 10757–10816.
[4] H. Chermette, *J. Comput. Chem.* **1999**, *20*, 129–154.
[5] J. K. Nørskov, T. Bligaard, A. Logadottir, S. Bahn, L. B. Hansen, M. Bollinger, H. Bengaard, B. Hammer, Z. Sljivancanin, M. Mavrikakis, Y. Xu, S. Dahl, C. J. H. Jacobsen, *J. Catal.* **2002**, *209*, 275–278.
[6] B. Hammer, J. K. Nørskov, *Surf. Sci.* **1995**, *343*, 211–220.
[7] H. Li, Y. Li, M. T. M. Koper, F. Calle-Vallejo, *J. Am. Chem. Soc.* **2014**, *136*, 15694–15701.
[8] A. A. Peterson, L. C. Grabow, T. P. Brennan, B. Shong, C. Ooi, D. M. Wu, C. W. Li, A. Kushwaha, A. J. Medford, F. Mbuga, L. Li, J. K. Norskov, *Top. Catal.* **2012**, *55*, 1276–1282.
[9] G. Mpourmpakis, A. N. Andriotis, D. G. Vlachos, *Nano Lett.* **2010**, *10*, 1041–1045.
[10] F. Calle-Vallejo, J. I. Martinez, J. M. Garcia-Lastra, P. Sautet, D. Loffreda, *Angew. Chem. Int. Ed.* **2014**, *53*, 8316–8319; *Angew. Chem.* **2014**, *126*, 8456–8459.
[11] F. Calle-Vallejo, J. Tymoczko, V. Colic, Q. H. Vu, M. D. Pohl, K. Morgenstern, D. Loffreda, P. Sautet, W. Schuhmann, A. S. Bandarenka, *Science* **2015**, *350*, 185–189.
[12] X. Ma, H. Xin, *Phys. Rev. Lett.* **2017**, *118*, 036101.
[13] N. Inoglu, J. R. Kitchin, *ACS Catal.* **2011**, *1*, 399–407.
[14] F. Abild-Pedersen, J. Greeley, F. Studt, J. Rossmeisl, T. R. Munter, P. G. Moses, E. Skúlason, T. Bligaard, J. K. Nørskov, *Phys. Rev. Lett.* **2007**, *99*, 016105.
[15] F. Calle-Vallejo, D. Loffreda, M. T. M. Koper, P. Sautet, *Nat. Chem.* **2015**, *7*, 403–410.

[16] M. Mavrikakis, B. Hammer, J. K. Nørskov, *Phys. Rev. Lett.* **1998**, *81*, 2819 – 2822.
[17] L. A. Kibler, A. M. El-Aziz, R. Hoyer, D. M. Kolb, *Angew. Chem. Int. Ed.* **2005**, *44*, 2080 – 2084; *Angew. Chem.* **2005**, *117*, 2116 – 2120.
[18] D. Balcells, E. Clot, O. Eisenstein, *Chem. Rev.* **2010**, *110*, 749 – 823.
[19] G. Jones, J. G. Jakobsen, S. S. Shim, J. Kleis, M. P. Andersson, J. Rossmeisl, F. Abild-Pedersen, T. Bligaard, S. Helveg, B. Hinnemann, J. R. Rostrup-Nielsen, I. Chorkendorff, J. Sehested, J. K. Norskov, *J. Catal.* **2008**, *259*, 147 – 160.
[20] S. Xie, S.-I. Choi, N. Lu, L. T. Roling, J. A. Herron, L. Zhang, J. Park, J. Wang, M. J. Kim, Z. Xie, M. Mavrikakis, Y. Xia, *Nano Lett.* **2014**, *14*, 3570 – 3576.
[21] A. A. Gokhale, J. A. Dumesic, M. Mavrikakis, *J. Am. Chem. Soc.* **2008**, *130*, 1402 – 1414.
[22] A. S. K. Hashmi, G. J. Hutchings, *Angew. Chem. Int. Ed.* **2006**, *45*, 7896 – 7936; *Angew. Chem.* **2006**, *118*, 8064 – 8105.
[23] A. Vojvodic, J. K. Norskov, F. Abild-Pedersen, *Top. Catal.* **2014**, *57*, 25 – 32.
[24] L. T. Roling, L. Li, F. Abild-Pedersen, *J. Phys. Chem. C* **2017**, *121*, 23002 – 23010.
[25] P. Giannozzi, S. Baroni, N. Bonini, M. Calandra, R. Car, C. Cavazzoni, D. Ceresoli, G. L. Chiarotti, M. Cococcioni, I. Dabo, A. Dal Corso, S. de Gironcoli, S. Fabris, G. Fratesi, R. Gebauer, U. Gerstmann, C. Gougoussis, A. Kokalj, M. Lazzeri, L. Martin-Samos, N. Marzari, F. Mauri, R. Mazzarello, S. Paolini, A. Pasquarello, L. Paulatto, C. Sbraccia, S. Scandolo, G. Sclauzero, A. P. Seitsonen, A. Smogunov, P. Umari, R. M. Wentzcovitch, *J. Phys. Condens. Matter* **2009**, *21*, 395502.
[26] B. Hammer, L. B. Hansen, J. K. Nørskov, *Phys. Rev. B* **1999**, *59*, 7413 – 7421.
[27] D. Vanderbilt, *Phys. Rev. B* **1990**, *41*, 7892 – 7895.
[28] *CRC Handbook of Chemistry and Physics* (Ed.: W. M. Haynes), CRC, Boca Raton, **2016**.
[29] L. Bengtsson, *Phys. Rev. B* **1999**, *59*, 12301 – 12304.
[30] H. J. Monkhorst, J. D. Pack, *Phys. Rev. B* **1976**, *13*, 5188 – 5192.

Manuscript received: November 16, 2017
Revised manuscript received: December 23, 2017
Accepted manuscript online: December 31, 2017
Version of record online: March 2, 2018